Appl. Phys. B 77, 409–414 (2003)
DOI: 10.1007/s00340-003-1261-0

Applied Physics B
Lasers and Optics

J. DEGALLAIX[1,✉]
C. ZHAO[2]
L. JU[1]
D. BLAIR[1]

Simulation of bulk-absorption thermal lensing in transmissive optics of gravitational waves detectors

[1] School of Physics, The University of Western Australia, Crawley, WA 6009, Australia
[2] Computer and Information Science, Edith Cowan University, Mount Lawley, WA 6050, Australia

Received: 4 March 2003/Revised version: 13 June 2003
Published online: 20 August 2003 •

ABSTRACT This paper presents finite-element modelling simulations of thermal lensing and thermal lens compensation in transmissive optics for gravitational wave detectors. We compare the current candidate test mass materials, fused silica and sapphire, in terms of sample geometry and time-dependent phenomena. For both materials, the thermal-lensing time constant is a few minutes, yet the core temperature needs several tens of minutes to stabilize. Thermal lens compensation using simple radiative heating is limited in temperature by absorption in the test mass. This effect limits the maximum allowed absorption for sapphire to $\sim$ 10–20 ppm/cm. For reasonable parameters, optical path length compensation within 1 nm can be achieved over a beam radius of 5 mm. If the optical absorption of the transmissive optics is too high, compensation can be achieved by means of a separate compensation plate.

PACS 42.25.Bs; 42.70.Ce

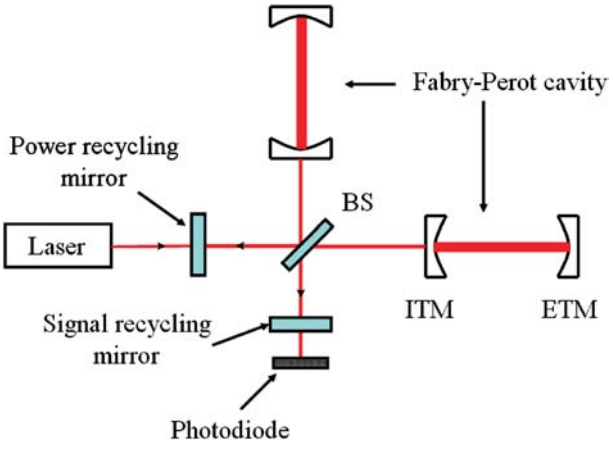

FIGURE 1 Principle of the gravitational wave detectors. BS, Beamsplitter; ITM, Input Test Mass; ETM, End Test Mass. For AIGO, the Australian project, the input power will be 50 W, the recycling cavity 3 kW and the arm cavity power 150 kW. In this simulation we studied the thermal lensing in the ITM. A similar effect occurs in the ETM (absorption coating of 1 ppm), but this effect is two orders of magnitude weaker than that in the ITM, and so can be neglected in the first approximation

1 Introduction

While cryogenic resonant bars have achieved impressive sensitivity to date, enormous efforts are underway to create laser interferometers detectors with broader bandwidth and even greater sensitivity. This technique is based on Michelson interferometers in which the arms consist of Fabry–Pérot cavities. The mirrors of the cavity are called "test masses" and are suspended to move freely, as shown in Fig. 1. A gravitational wave passing through the interferometer changes the relative length of the two arms, creating a variation in the current from the photodiode. Both power and signal recycling [1] techniques are used to increase the circulating optical power and so improve the sensitivity of the interferometer.

Advanced interferometers represent substantial upgrades of the original LIGO [2] and VIRGO [3] interferometers now being tested. They are planned to achieve spectral strain sensitivities of $\sim 10^{-22}$. The reduction of the high-frequency detection limit due to shot noise by increasing the optical power until its magnitude is comparable to the radiation pressure noise has been proposed. This corresponds to several kW of circulating power passing through the beamsplitter. Unfortunately, high-power lasers and recycling cavities lead to some undesirable effect such as thermal lensing. The weak absorption of the test masses causes an induced refractive index change within the material, resulting in a wavefront distortion.

An analytical solution of thermal lensing in optical materials has been calculated by Hello and Vinet [4], for both steady-state and transient cases. Winkler et al. [5] have suggested a simple and robust model of heating by optical absorption and have reported its consequences on the performance of an interferometer. To limit the effect of thermal lensing, different optical configurations were tested by Strain et al. [6]. Lawrence et al. [7] have explored adaptive thermal compensation with Melody/Matlab [8] simulations to correct optical path length changes. Lück [9] has achieved the first experiment of wavefront correction by a scanning laser. Finally Beausoleil [10] has developed a specialized code "Melody" to model the thermal wavefront distortion in a whole interferometer.

The two current candidates for test mass materials are fused silica and sapphire. Fused silica is being used in the first generation of interferometers. Sapphire is preferred for

✉ Fax: +61-8/9380-1170, E-mail: etudeohp@cyllene.uwa.edu.au

its mechanical properties [11] for advanced interferometers. However it still has problems with optical homogeneity, anisotropy, and absorption, especially in large samples. The parameter that determines the magnitude of thermal lensing in a material is the ratio $\zeta = \beta a/k_{\mathrm{th}}$, where β is the thermo-optic coefficient, a the absorption, and k_{th} the thermal conductivity. For fused silica and sapphire, ζ is similar (relative difference of 4%), which means that thermal lensing will be of almost the same order. However, the time evolution and correction of the thermal lens will be vastly different. A high thermal conductivity guarantees a rapid equilibrium, while the absorption, which is more than 20 times higher for sapphire than for fused silica, determines the final temperature.

In this paper we present an analysis of thermal lensing and thermal lens compensation by means of a widely used Finite Element Modelling (FEM) package. Compared with Melody, the software used here can naturally handle 3-dimensional geometries. Thus, complex thermal lens compensation and non-axisymmetric perturbations (such as in the suspension system) can be easily included. The FEM method used here is particularly useful for determining the temperature evolution of the test masses. By considering widely differing test mass geometries, we obtain an insight into the role of the geometry, which could influence future choices of test mass dimensions.

The Australian Consortium for Interferometric Gravitational Astronomy (ACIGA), in collaboration with the US LIGO project, is currently planning to test very high optical power Fabry–Pérot cavities using sapphire test masses in its Gingin research facility. Because of the relatively large absorption observed in most sapphire samples, it is mandatory to use a thermal lens compensation scheme. Hence, in the last section of this paper, we study the performance of the simplest thermal lens compensation device, a radiative heating ring.

2 FEM of thermal lensing

Finite element modelling is useful because of its ability to manage irregular shapes and inhomogeneous or anisotropic materials. Here we explain the application of FEM to thermal-lensing problems. We include both thermal conduction and radiation to determine the temperature profile inside an optical component due to a laser beam.

2.1 *FEM approach*

To describe thermal lensing inside the material, we need to handle the heat equation with non-uniform heating, because of the Gaussian shape of the laser beam and the radiative process on the surface. A direct calculation is very tedious and has already been done [4]. We used a numerical simulation based on finite element theory to determine the dynamic behavior of the optics. This method has been successfully used to solve complex mechanics problems over the last 20 years, and is also well adapted to heat problems. The basic principle is to divide a complex shape into a large number of simple elements, such as triangles or quadrilateral, defined by their nodes. After the discretization stage, each node's properties (e.g., temperature) are linked to its neighbor's by a polynomial interpolation characterizing the physical equations (e.g., heat conduction and thermal radiation) and the boundary conditions, forming an approximate system of equations for the whole structure. Then the system of equations involving the unknown quantities at each node is solved numerically. We only made one assumption: the sample is effectively opaque to thermal radiation and has an emissivity of 1 [12]. This is a very good assumption as long as the thermal radiation temperature is less than 650 K.

The simulation was performed with the software ANSYS 6.1. We discretized the sample into more than 25 000 nodes using an automatic meshing. The radiation solver used an iterative method and the tolerance for the solution was set at 10^{-8}. The method and results were verified by comparison with an analytic model [4]. The simulation results fit well with the theory with an error of less than 1% within the waist of the laser beam.

2.2 *Setup*

We modeled a 1 kW Gaussian beam of waist[1] $w = 5$ mm passing through two different test masses: (A) a 10 cm long cylinder with a radius of 1.5 cm (suitable for many evaluation samples), and (B) a 6 cm long cylinder with a radius of 15 cm (comparable to medium-scale test masses planned for use at Gingin). We chose the value 1 kW, as it corresponds to the typical power level expected in power recycling cavities. The materials considered were fused silica and sapphire initially at 300 K. The material properties used in this simulation are summarized in Table 1. We note that the absorption figures used here do not represent the best values possible. Fused silica with an absorption of less than 1 ppm/cm is available. Some samples of sapphire have been observed with absorptions less than 10 ppm/cm [14].

To determine the optical path length across the crystal, we need not only the temperature distribution, but also the photoelastic effect and the thermal expansion at each end [15]. However, the contributions to the changes of the refractive index due to the increase of temperature dominate, as shown in Table 2. We therefore only deal with the latter in this article.

Material	Absorption (ppm/cm)	$\mathrm{d}n/\mathrm{d}T$ (10^{-6} K)	k_{th} (W/mK)	C (J/kg K)	ϱ (kg/m^3)	α (10^{-6} K)
Fused silica	2	10	1.38	746	2202	0.55
Sapphire	50	13	46	777	3987	5

TABLE 1 Parameters of the optical materials used [13]

Material	$\Lambda_{\mathrm{thermal}}$ (nm)	$\Lambda_{\mathrm{stress}}$ (nm)	$\Lambda_{\mathrm{expansion}}$ (nm)
Fused Silica	15	–0.34	0.12
Sapphire	15	0.47	1.1

TABLE 2 Contributions of the different effects to the optical path length changes for the A-geometry sample. $\Lambda_{\mathrm{thermal}}$ represents the effect of the temperature rise, $\Lambda_{\mathrm{stress}}$ the photoelastic effect, and $\Lambda_{\mathrm{expansion}}$ the thermal expansion. The results for geometry B are of the same order

[1] distance from the beam center at which the beam intensity has fallen of $1/\mathrm{e}^2$ of its peak value

3 Results

Below we present data on the temperature evolution of the test mass core. The results show an interesting difference between the time constants for the core temperature and for thermal lensing. The core temperature takes many hours to come to equilibrium, while the thermal lensing mainly equilibrates in less than five minutes for both geometries.

3.1 *Temperature evolution*

For the A-geometry (small cylinder), the core temperature inside sapphire only stabilizes to about 307 K after about 3 hours. The time constant τ (time at which 63% of the equilibrium temperature is reached) is 32 min. For fused silica, which has a lower optical absorption, the final temperature is 300.3 K and the time constant is 19 min (see Fig. 2). The evolution of temperature for the B-geometry is different. The equilibrium is again reached earlier for fused silica ($\tau = 11$ min) than for sapphire ($\tau = 91$ min). We noticed, however, that the change in geometry leads to a decrease in the time constant for fused silica and an increase for sapphire. This behavior occurs mainly due to the difference between the thermal conductivities of these materials. To reach equilibrium, the fused silica test mass predominantly radiates the absorbed heat from hot spots on the two sides of the cylinder. The cylinder walls do not radiate, because they remain cool due to the low thermal conductivity of fused silica. Because of its high thermal conductivity, the sapphire test mass avoids having localized hot surface and equilibrium is only reached when all the areas of the test mass reach the average value of 300.1 K, which takes a longer time. For the B-geometry and for both materials, the final temperatures are lower. This improvement is due to the large radius of the sample. The heat produced in the middle is cleared by conduction inside the cylinder and the large surface of the optics ensures efficient cooling by radiation.

The simulation was only performed with an input optical power of 1 kW, but we can already foresee some problems for the A-geometry if the power were to be increased to 50 kW, as could happen in the recycling cavities of the next generation of interferometers. After a long stabilization (several hours), the temperature inside the sapphire would exceed 450 K. The deformation of the material could become critical and compensation schemes could be impossible.

3.2 *Optical path length dynamic*

For the characterization of thermal lensing, we define Δ_{OPL} as the difference of the optical path length between the center and the waist w of the Gaussian beam. Thanks to the symmetry of the material, the temperature inside the cylinder depends only on the radius r and the distance z from one side, so $T(r, \theta, z) = T(r, z)$. Thus we can write

$$\Delta_{\mathrm{OPL}} = \beta \int_0^L \left[T(w, z) - T(0, z)\right] \mathrm{d}z \tag{1}$$

where $\beta = \mathrm{d}n/\mathrm{d}T$ is the thermo-optic coefficient and L is the length of the cylinder. The plots of $\Delta_{\mathrm{OPL}}(t)$ for fused silica and sapphire are shown in Fig. 3 for both test mass sizes. Although the absorption of sapphire is more than twenty times greater than that fore fused silica, the thermal lensing in this material is of the same order, due to its high thermal conductivity. High conductivity, by equalizing the temperature faster,

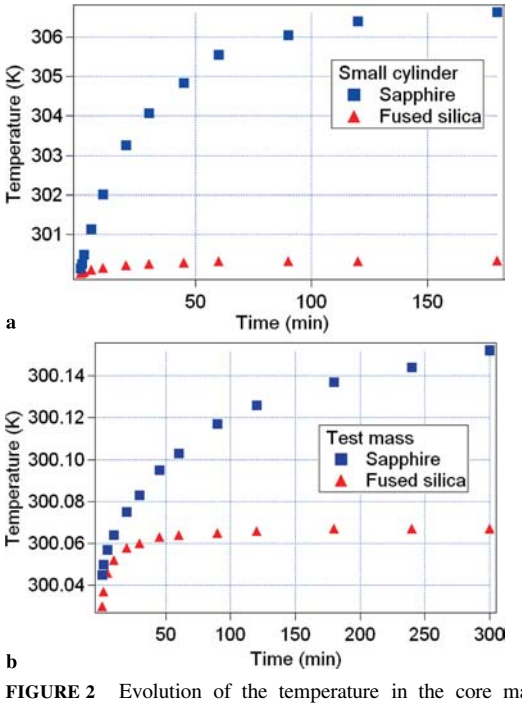

FIGURE 2 Evolution of the temperature in the core materials (hottest point) versus time for the small cylinder (**a**) and for the real test mass (**b**). The input laser beam has a power of 1 kW

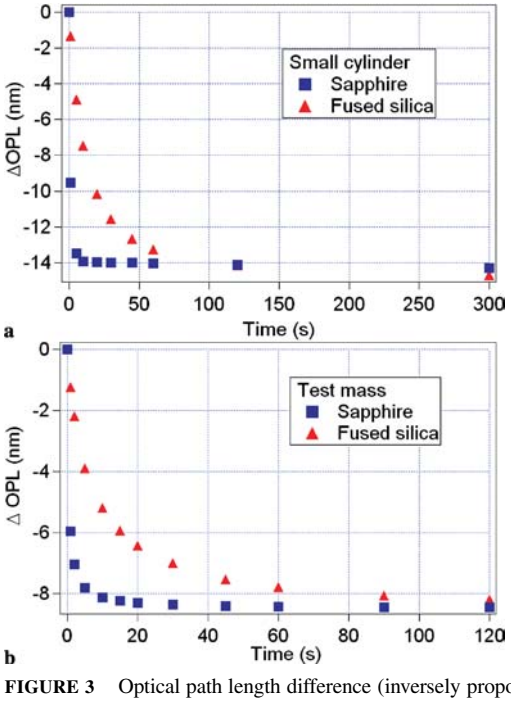

FIGURE 3 Optical path length difference (inversely proportional to the focal length) versus time for fused silica and for sapphire for both geometries (A and B). The input optical power is 1 kW

limits the optical path distortion. Moreover, it allows thermal equilibrium to be reached faster, making closed loop corrections more effective. The time constant for the thermal lens is much shorter than for the temperature distribution. For both geometries, equilibrium is always reached in less than 5 min for fused silica, while sapphire takes 2 min. As shown by (1), the optical path distortion is directly proportional to the length of the cylinder. Thus, a shorter cylinder is more advantageous with regards thermal lensing.

4 Thermal lens compensation

In high-power interferometers, thermal lensing results in the reduction of the contrast and can possibly cause cavities to become unstable [6]. Thus thermal lensing limits the maximum optical power in the arms of an interferometer. Correcting this effect is indispensable if the expected sensitivity goals are to be reached.

4.1 *Thermal compensation*

The main method to limit thermal lensing is to reduce the thermal gradient inside the optics. This scheme has been investigated by Ryan Lawrence, Mike Zucker, and the LIGO team at MIT. They have proposed the use of heating rings for axial compensation and a scanning CO_2 laser (first demonstrated by Lück [9]) for adaptive correction [7]. In this paper, we considered only a simple heating-ring compensator device close to the material, which heats the sample by radiation. Physical contact, although more efficient for heat transfer, is not considered because it degrades the thermal noise of the test mass.

To have a meaningful effect, the expected temperature of the heater needs to reach 600 K. For radiation at this temperature, the optics are opaque and a calculation of the penetration depth [16] reveals that 90% of the radiation is absorbed in the first 13 mm for fused silica and 8 mm for sapphire. The temperature of the heater is regulated by observing the wavefront distortion. A positive focal value of the thermal focal lens requires an increase in the heater's temperature.

4.2 *Small optics*

We first present thermal compensation results for the small samples (A-geometry) introduced in the previous section. The heating device is a cylinder of 40 mm length with a radius of 20 mm, as shown in Fig. 4a. By studying the optical path difference versus the temperature of the heater, the existence of an optimal temperature is predicted. To characterize the quality of the correction, we define a weight function expressing the importance of the center of the Gaussian beam, at which the energy is concentrated relative to its edges. We define the function of error M_{OPL} as

$$M_{\mathrm{OPL}} = \int_0^{R_c} \left(\beta \int_0^L [T(r,z) - T(0,z)] \mathrm{d}z \right)^2 \mathrm{e}^{-2(r/w)^2} \mathrm{d}r \qquad (2)$$

where R_c is the radius or the cylinder. The plot of this function versus the temperature of the heating ring is shown in Fig. 5. As expected, we found an optimal temperature, indicated by

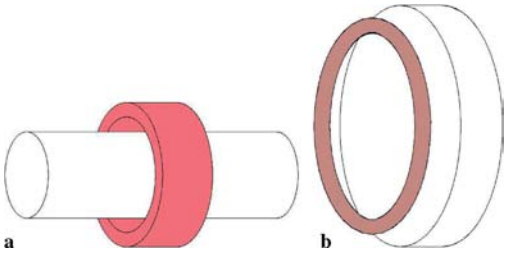

FIGURE 4 Position of the heating ring (*shaded part*) for small optics (**a**) and for the current test masses (**b**)

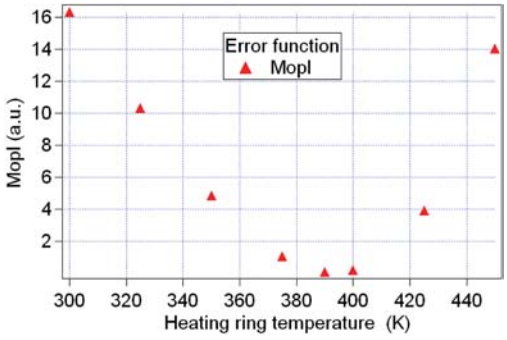

FIGURE 5 Function of error versus temperature of the heating ring for the A-geometry fused-silica optics. The most suitable temperature is determined by the minimum of this function. In this case, the 40 mm long heating ring is placed in the middle of the sample at a distance of 5 mm from its surface

a minimum in the thermal-lensing error function. This temperature is 390 K for fused silica. For sapphire, in order to increase the efficiency of the correction, the length of the heating cylinder is 10 cm (same length as the optic). In this case, the optimal temperature of the heater is 580 K. The high heating temperature required for sapphire is a consequence of its higher absorption, which sets its core temperature. Moreover, sapphire's high thermal conductivity reduces the thermal lens magnitude, as well as the efficiency of the correction, by smoothing the temperature distribution. After correction, the optical path difference is reduced by more than 80% within the waist.

4.3 *Large optics*

Although a cylindrical ring is suitable for thermal compensation for the A-geometry, this solution is not effective for the B-geometry due to the much larger dimensions (radius of 150 mm with length of 60 mm). It is extremely difficult to achieve the required thermal gradient in the center of the sample due to the larger diameter of the cylinder. It is especially difficult for sapphire because of its high thermal conductivity. One solution is to place a toroidal heating ring in front of the sample, as shown in Fig. 4b. To determine the minimum correction temperature, we optimized the radius of the heating ring. In Fig. 6, we plot the induced focal length due to the heating ring (without the laser beam) versus the ring radius. The minimum focal length is found for a ring diameter 0.8 times the diameter of the optics. The diffraction due to the heating ring could be neglected, because the aperture is 20 times greater than the waist of the laser.

The heating ring dimensions will be used for the first test of the Australian high-optical-power facilities in Gingin. For

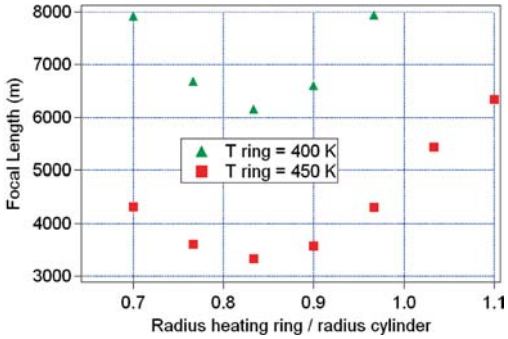

FIGURE 6 Thermal focal length induced by the heater (without the laser beam) versus its diameter for two temperatures and after one hour for the sapphire test mass. The torus, of outer minor radius 10 mm, is placed 10 mm from the cylinder's end. The minimum of the curve represents the maximum efficiency of the heater in compensating for the effect of the laser beam

an advanced interferometer, the diameter of the ring will need to be the same as that of the test mass so as not to reduce the clear aperture of the mirror.

Using the same error function defined by (2), we determined the optimal heating temperature for minimum optical path distortion to be 490 K for fused silica and more than 900 K for sapphire. These temperatures are high because of the inefficient radiative heating process. Moreover, the transparency window of sapphire begins at 5 μm, and some radiation from the heating ring above 650 K is not locally absorbed by the material. Thus this method of correction is most efficient if the total absorbed optical power is lower than assumed here. One solution is to use another heating ring on the other side of the sample. It could be possible to add reflectors around the heater to focus the radiation. A small reduction in temperature can also be achieved by increasing the size of the heating ring.

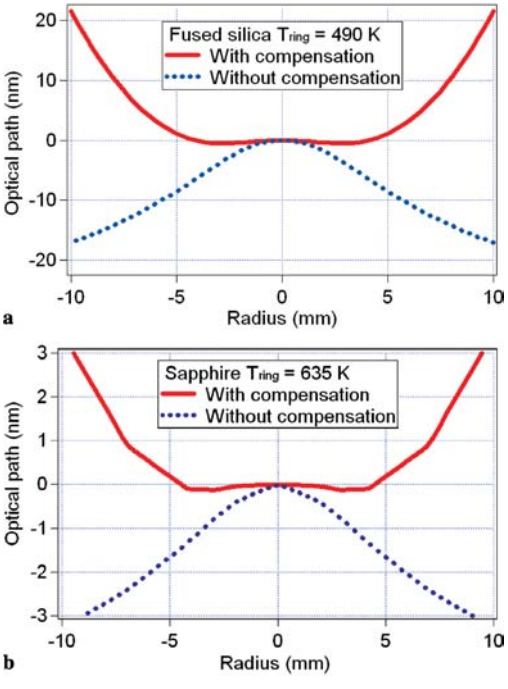

FIGURE 7 Comparison between the optical path length difference with and without the thermal compensation. The plots are for the B-geometry and for both silica and sapphire. For sapphire, we assumed an absorption of 10 ppm/cm to allow for the compensation by the heating ring

The optimal temperature of the heating ring is 490 and 635 K, respectively, for fused silica and sapphire, with an absorption of 10 ppm/cm. The average core temperature for the fused-silica optics is 310 K, with the hot points (located on the surface of the optics just in front the heating ring) at 322 K. For sapphire, its higher thermal conductivity allows a more uniform temperature, thus the average temperature is 333 K and the hot points are at 334 K.

Thermal compensation results are shown in Fig. 7. According to the optical path length difference, the correction for the sapphire (assuming an absorption of 10 ppm/cm) is six times greater than that for fused silica. For fused silica, we achieved an optical path length difference of less than $1.2 \times 10^{-3}\lambda$ within 5 mm. For sapphire, we reach $2 \times 10^{-4}\lambda$ within the waist.

Distortions resulting from the thermal lens lead to the conversion of light from the fundamental mode TEM_{00} to higher order spatial modes [15]. Thanks to the heating ring, the mode power conversion could be divided by four for both fused silica and sapphire.

4.4 *Comments*

In this article, in order to simplify the calculations, the thermal lensing simulations did not include substrate mechanical deformations. The substrate mechanical expansion contribution to the optical path length difference was assumed to be negligible compared with the contribution of the thermo-optic effect (as shown in Table 2). To confirm this assumption, we include in this section the material thermal expansion in our simulation for the B-geometry, the medium-scale test mass. The new trends of the results are different for fused silica and sapphire, mainly due to sapphire's thermal expansion coefficient being ten times larger than that of fused silica. Without the compensation scheme, the optical path length difference is increased by 2% for fused silica and 10% for sapphire. The change in the sagitta δs, measured across the beam diameter, is 0.065 nm for fused silica and 0.67 nm for sapphire. This deformation increases the mirror convexity. However, the heating ring induces an opposite change to the mirror curvature, as shown in Fig. 8. The compensation scheme inverts the temperature gradient inside the optics, so the mechanical deformation in this situation increases the mirror concavity. For the optimal heating ring temperatures of Sect. 4.3, δs equals −0.38 nm for fused silica and −0.65 nm for sapphire. This thermal expansion can partially counter-balance the thermal lensing from the substrate for the sapphire test mass. Thus, the required heating ring temperature to minimize wavefront distortions is reduced from 635 to 550 K.

Previous models [4, 12] of thermal lensing have used the assumption of small variations of temperature in the optics. This simplification allows faster calculations by linearizing the radiation heat exchange equation (e.g., $T_{\mathrm{TM}}^4 - T_0^4 \sim 4(T_{\mathrm{TM}} - T_0)T_0^3$). For compensation by a heating ring, the temperature difference between the test mass and its surrounding could exceed 40 K. In this case, the linear extrapolation is no longer valid, and leads to an error of 15% in the radiated

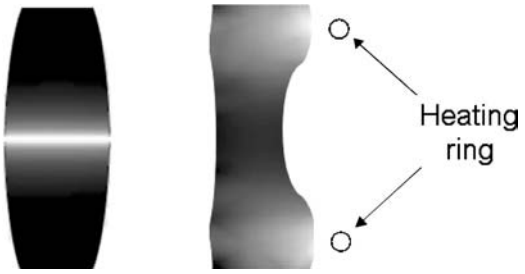

FIGURE 8 Exaggerated mechanical deformation for the sapphire test mass without (*left*) and with (*right*) thermal compensation. The temperature cross-sections of the samples are also represented, with *lighter shading* indicating hotter regions of the optics. The temperature gradient in the left and right samples are 0.06 and 3 K, respectively

power. In all the simulations presented in this article, the exact model of radiation heat transfer is used.

The heat that is required to correct the thermal lens is strongly dependent on the size of the beam. The simulation in this paper refers to the high-optical-power laser experiments in AIGO, which themselves represent a reduced-scale version of the proposed advanced LIGO. For the parameters used in this paper, except for a beam waist size increased to 6 cm (like planned for LIGOII), and for a sapphire test mass with an absorption of 50 ppm/cm, the results are substantially different from the results presented here. In the large waist situation, the optimal temperature of the heating ring is greatly reduced to 330 K. Thus, the compensation by means of a heating ring is practicable, and can be achieved by radiating only 5 W.

In the simulations presented here, the limitation of the heating-ring compensation scheme is the transparency window of the sapphire. In an advanced LIGO type interferometer, the greatest constraint comes from the allowable temperature of the test mass. A significant temperature rise in the test mass optics introduces creep into the mechanical isolation system, as well as increased thermal noise.

5 Conclusion

We have presented a numerical technique that allows the accurate estimation of thermal lensing in transmissive optics. The FEM method confirms the time dependence previously expected from analytical estimates and shows that thermal lensing is strongly dependent on the test mass geometry. Our results show that test masses take many hours to reach thermal equilibrium in almost all thermal lensing situations. The thermal lensing time constant can be much smaller, at less than 5 min for both sapphire and fused silica. For the geometries investigated, thermal lensing can be effectively compensated to within $\lambda/1000$ over a beam radius of 5 mm.

Compared with fused silica, sapphire requires a higher temperature for the heating ring to obtain good compensation, because its absorption is higher. One drawback of sapphire is the larger transparency window compared with silica, which limits the temperature radiation from the heater. However, when a new generation of sapphire with lower absorption is available, we expect that the temperature of the heating ring could be reduced substantially.

To correct strong thermal lensing in relatively high-absorption materials, it appears that the only feasible option is to have a separate fused-silica compensation plate. This solution required 20 times less power if the heating is applied by conduction instead of radiation, and avoids the direct heating of the test mass. However, high-performance AR coating of the plate is essential and thermal noise can become a serious issue.

In this simulation we studied the case of a single test mass. A complete simulation should include the thermal expansion of the material in addition to the thermo-optic effect. The next step in our simulation studies will combine these effects and will be applied to a complete optical cavity. Thus we will directly simulate the power coupling and contrast defects resulting from thermal lensing and determine their consequences for the performance of the interferometer. In future work, we will also use the FEM method to model test masses that include suspension elements and other non-radially symmetric perturbations. The strong dependence on test mass geometry also requires further investigation to determine the optimum test-mass configuration.

ACKNOWLEDGEMENTS The authors would like to thank the International Advisory Committee of the ACIGA/LIGO High Power Project for their encouragement and advice, and particularly Ryan Lawrence and the LSC reviewers for their comments on this manuscript. This research was supported by the Australian Research Council and the Department of Education, Science and Training. It is a project of the Australian Consortium for Interferometric Gravitational Astronomy in collaboration with the LIGO project.

REFERENCES

1 D.E. McClelland: Aust. J. Phys. **48**, 953 (1995)
2 A. Abramovici, W.E. Althouse, R.W.P. Drever, Y. Gursel, S. Kawamura, F.J. Raab, D. Shoemaker, L. Sievers, R.E. Spero, K.S. Thorne, R.E. Vogt, R. Weiss, S.E. Whitcomb, M.E. Zucker: Science **256**, 325 (1992)
3 C. Bradaschia, R. Del Fabbro, A. Di Virgilio, A. Giazotto, H. Kautzky, V. Montelatici, D. Passuello, A. Brillet, O. Cregut, P. Hello, C.N. Man, P.T. Manh, A. Marraud, D. Shoemaker, J.Y. Vinet, F. Barone, L. Di Fiore, L. Milano, G. Russo, J.M. Aguirregabiria, H. Bel, J.P. Duruisseau, G. Le Denmat, Ph. Tourrenc, M. Capozzi, M. Longo, M. Lops, I. Pinto, G. Rotoli, T. Damour, S. Bonazzola, J.A. Marck, Y. Gourghoulon, L.E. Holloway, F. Fuligni, V. Iafolla, G. Natale: Nucl. Instrum. Methods Phys. Res. A **289**, 518 (1990)
4 P. Hello, J.Y. Vinet: J. Phys. (France) **51**, 1267 (1990)
5 W. Winkler, K. Danzmann, A. Rüdiger, R. Schilling: Phys. Rev A **44**, 7022 (1991)
6 K.A. Strain, K. Danzmann, J. Mizuno, P.G. Nelson, A. Rüdiger, R. Schilling, W. Winkler: Phys. Lett. A **194**, 124 (1994)
7 R. Lawrence, M. Zucker, P. Fritschel, P. Marfuta, D. Shoemaker: Class. Quantum Grav. **19**, 1803 (2002)
8 R.G. Beausoleil: 'Melody/Matlab object-oriented model of gravitational-wave interferometers using Matlab'. Technical report no. G020165-00-Z, Ligo (2002)
9 H. Lück, K.-O. Müller, P. Aufmuth, K. Danzmann: Opt. Commun. **175**, 275 (2000)
10 R.G. Beausoleil, E.K. Gustafson, M.M. Fejer, E. D'Ambrosio, W. Kells, J. Camp: J. Opt. Soc. Am. B **20**, 1246 (2002)
11 M. Taniwaki, L. Ju, D.G. Blair, M.E. Tobar: Phys. Lett. A **246**, 37 (1998)
12 R. Lawrence, M. Zucker, P. Fritschel, P. Marfuta, D. Shoemaker: 'Active wavefront correction in laser interferometric gravitational waves detectors'. Technical report no. T010056-00-R, Ligo (2001)
13 F. Benadid: 'Optical properties of sapphire test mass in laser interferometric gravitational wave detectors'. PhD thesis, University of Western Australia (2000)
14 D. Blair, F. Cleva, C.B. Man: Opt. Mater. **8** 233 (1997)
15 J.D. Mansell, J. Hennawi, E.K. Gustafson, M.M. Fejer, R.L. Byer, D. Clubley, S. Yoshida, D. Reitze: Appl. Opt. **40**, 366 (2001)
16 R.D. Guenther: *Modern Optics* (Wiley, New York 1990)